Supplementary information

Electrically modulated relaxation dynamics of pre-stretched droplets post switched-off uniaxial extensional flow

Nalinikanta Behera[a], and Suman Chakraborty[*a]

[a]Department of Mechanical Engineering, Indian Institute of Technology Kharagpur, Kharagpur,West Bengal-721302, India

1 Validation of the numerical method

In this compare the present numerical results with the reported benchmark results on droplet dynamics in uniaxial extensional flow [1,2] and uniform electric field[3], respectively. The flow limits in the above studies correspond to the Stokes regime. To simulate the Stokes flow regime, we consider Re=0.01 in our numerical code. In Fig. S1a, we present the influence of extensional flow on steady-state droplet deformation for λ=1. Here, the electric field is absent (Ca_E=0). For this study, we have compared our results with the reported numerical results of Stone & Leal [1]. The droplet deformation is quantified by the parameter $D=(L-B)/(L+B)$, where L and B are the half-length of droplet along the z-axis (i.e. outward flow direction) and transverse direction, respectively (see the inset of Fig. S1a). With the increase in Ca, the strength of the viscous stress as compared to the capillary stress enhances, augmenting the deformation as facilitated by the imposed stretching. Evidently, the deformation predicted by our numerical model matches well with the numerical results of Stone & Leal [1]. In Fig. S1b, we next compare the temporal elongation and relaxation of a droplet as obtained from the present simulations with the reported experimental results of Ha & Leal [2], considering λ=0.056, and the Capillary number just above the critical value i.e. Ca_c. Here, $t^*\left(=\overline{t}G\right)$ is the dimensionless time. The flow is stopped at L=4.3. From Fig. S1b, it is evident that the evolution of the droplet shape during elongation and relaxation (provided in the inset) phases are well predicted by the present numerical model. Moreover, an excellent match is observed in terms of the observed breakup modes. However, the critical Capillary number found in the present study is slightly higher (Ca_c=0.194) as compared to the experimental value (Ca_c=0.178).

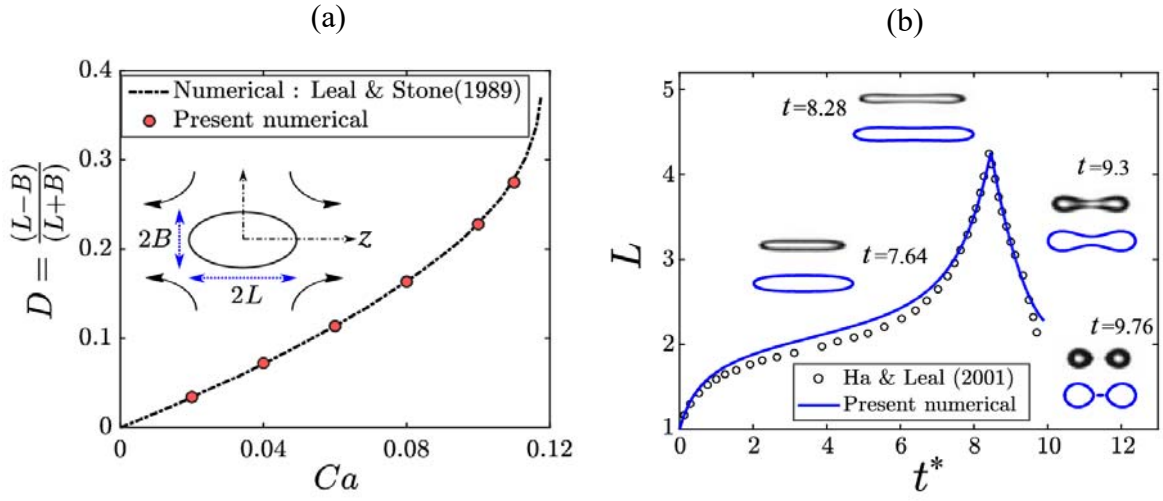

Fig. S1 (a) Effect of capillary number, Ca, on the steady-state deformation parameter D for λ =1. (b) Transient variation in the droplet half-length L in the presence of extensional flow and after the flow is stopped for λ=0.056 and Ca=1.05Ca_c, where the critical capillary number, Ca_c=0.195. The value of Reynolds number is taken as Re=0.01, both for figures (a) and (b).

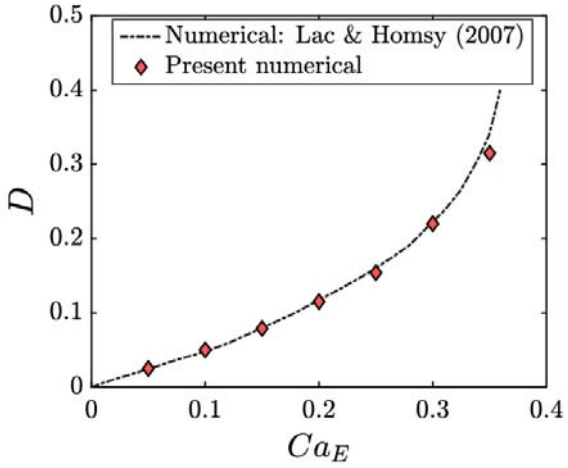

Fig. S2 Deformation parameter as a function of electric capillary number, Ca_E, for (R, S, λ) = (10, 1.37, 1). The value of Reynolds number is taken as Re=0.01.

Next, we assess the present numerical model in predicting the droplet deformation in the sole presence of electric field. Fig. S2 depicts the deformation (D) as a function of electric capillary number (Ca_E) for (R, S, λ) = (10, 1.37, 1) in the Stokes flow limit. Our numerical simulations show prolate deformation (D>0) for this set of fluid properties. An increase in Ca_E augments the relative strength of the electric stress with respect to the capillary stress, which reflects enhanced

deformation. The results obtained by the numerical model agree very well with the numerical results of Lac & Homsy [3], as depicted in Fig. S2.

2 Grid and domain independence tests

Throughout our study, we have used a complex grid structure that is refined to level 10 (where level m corresponds to a grid size $\Delta x = \Delta z = H \times 2^{-m}$) at the fluid-fluid interface and refined to level 6 at far away from the drop. However, during the transient process, the grids near the high curvature zone on the interface can be further divided into level 11 due to the implementation of curvature-based refinement in the numerical model. Hence, there is non-uniformity in grid size at the interface as shown in Fig. 2b of the main text. To conduct the grid independence test, we perform simulations using uniform grid refinement levels 10 and 11 at the interface, and compare the results with the same obtained by the present grid structure, whereas, the grid size in the bulk medium is kept unaltered. Figure S3a shows the evolution of the drop for (R, S, λ) = (10,1.37,1), considering Ca=0.12 and Ca_E=0.3, Re=0.01, taking different grid structures. It can be seen that by refining the grid size from level 10 to 11, the transient deformation and the breakup mode (provided in the inset) remain nearly unaffected. Therefore, for the sake of computational time optimization as well as to capture the evolution of the neck with uncompromised accuracy, the present curvature-adaptive grid structure is used. Figure S3b depicts the transient length variation considering the previous set of parameters, for two different domain sizes: H=15 and H=30 (corresponding widths are W=30 and W=60, respectively). From figure S3b, it is clear that increase in the domain size has negligible effect on the transient drop dynamics. Hence, for simulation purposes, we have used the domain size $H \times W$=15×30.

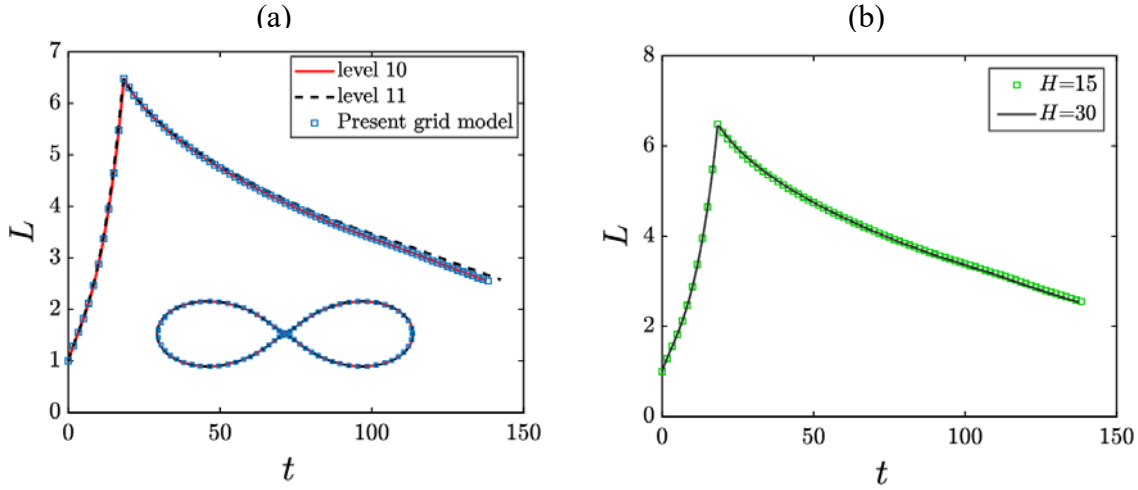

Fig. S3 (a) Transient deformation of the drop for different grid sizes. The inset shows comparison between the break-up modes. (b) Effect of domain size on transient deformation. The system under consideration is (R, S, λ)=(10, 1.37 ,1). To obtain the bulbous-ended base state, (Ca_E, Ca)= (0.3, 0.12) is taken in pre-relaxation stage.

3 Mathematical modeling of necking

Fig. S4 shows the schematic of a relaxing drop with bulbous ends connecting to a relatively thin neck. For theoretical analysis, we consider a cylindrical coordinate system (r, z) with origin at the drop center. In Stokes flow limit, the Navier-Stokes in the z-direction is written as

$$\frac{1}{\lambda}\frac{\partial p}{\partial z}=\frac{\partial^2 u_z}{\partial z^2}+\frac{1}{r}\frac{\partial}{\partial r}\left(r\frac{\partial u_z}{\partial r}\right). \tag{1}$$

Few assumptions and simplifications are made to solve the above equation. The size of the neck is assumed to be significantly small compared to drop size i.e. $w/L<<1$, consequently,

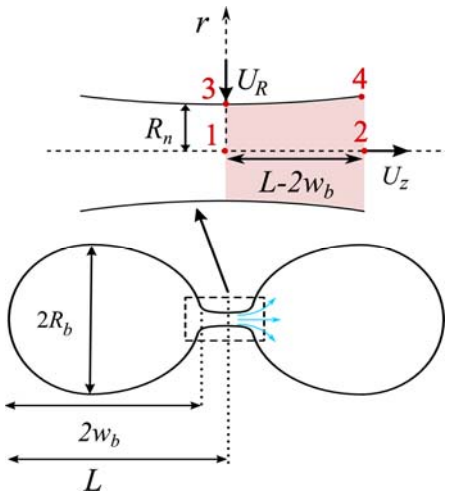

Fig. S4 Schematic of neck present two bulbous ends of a relaxing drop

$\partial^2 u_z/\partial z^2 << \partial^2 u_z/\partial r^2$ is also valid. Neglecting $\partial^2 u_z/\partial z^2$ from eqn (1) and integrating the rest of the terms with respect to r between point 2 and point 4, we obtain

$$u_z\big|_2=\frac{R_n^2}{4\lambda\left(L-2w_b\right)\left(1-\alpha\right)}\left(p_1-p_2\right), \tag{2}$$

where $\alpha=u_z\big|_2/u_z\big|_4$. Due to the lack of priori knowledge about α, we take the help of our numerical observations to proceed further. In all of the considered cases it is observed that $\alpha\sim O\left(10^{-1}\right)$, thus, by neglecting α in the denominator of eqn (2), one can still get the approximate results. Now, to calculate the radial velocity term, we integrate the continuity equation, $\partial u_z/\partial z+\partial u_r/\partial r+u_r/r=0$ between point 1 and 3, and plugging the results into eqn (2) , we obtain

$$u_r\big|_3 = \frac{\partial R_n}{\partial t} = -\frac{R_n^3}{4\lambda\left(L-2w_b\right)^2}\left(p_1 - p_2\right). \tag{3}$$

The pressures inside the neck (or meniscus) and at the entrance to the bulbous-ended structures can be calculated as $p_1 \sim 1/R_n - 1/\left(L-2w_b\right)$ and $p_2 \sim \left(1/R_b + 1/w_b\right)/2$. Approximating the bulbous structures as ellipsoids and knowing that the total drop volume is the summation of the volume of neck and bulbous structure, the length of semi major axis can be calculated as,

$$R_b = \sqrt{\left(\frac{2}{3} - R_n^2(L-2w_b)\right)\frac{3}{4w_b}}\,. \tag{4}$$

References

1 H. A. Stone and L. G. Leal, *J. Fluid Mech.*, 1989, **198**, 399.

2 J.-W. Ha and L. G. Leal, *Phys. Fluids*, 2001, **13**, 1568–1576.

3 E. Lac and G. M. Homsy, *J. Fluid Mech.*, 2007, **590**, 239–264.